

Strain rate effects on pressure-induced amorphous-to-amorphous transformation in fused silica

Wenhao Song(宋文豪), Bo Gan(甘波), Dongxiao Liu(刘东晓), Jie Wu(吴杰), Martin T. Dove, and Youjun Zhang(张友君)

Citation: Chin. Phys. B, 2025, 34 (**4**): 046101. DOI: 10.1088/1674-1056/adb38f
Journal homepage: http://cpb.iphy.ac.cn; http://iopscience.iop.org/cpb

What follows is a list of articles you may be interested in

Atomic origin of minor alloying element effect on glass forming ability of metallic glass

Shan Zhang(张珊), Qingan Li(李庆安), Yong Yang(杨勇), and Pengfei Guan(管鹏飞)
Chin. Phys. B, 2025, 34 (**3**): 036105. DOI: 10.1088/1674-1056/ada756

Quasi-plastic deformation mechanisms and inverse Hall-Petch relationship in nanocrystalline boron carbide under compression

Zhen Yue(岳珍), Jun Li(李君), Lisheng Liu(刘立胜), and Hai Mei(梅海)
Chin. Phys. B, 2024, 33 (**8**): 086105. DOI: 10.1088/1674-1056/ad4989

Residual stress modeling of mitigated fused silica damage sites with CO_2 laser annealing

Chuanchao Zhang(张传超), Wei Liao(廖威), Lijuan Zhang(张丽娟), Xiaolong Jiang(蒋晓龙), Zhenhua Fang(方振华), and Xiaodong Jiang(蒋晓东)
Chin. Phys. B, 2024, 33 (**3**): 036101. DOI: 10.1088/1674-1056/acf447

Strain rate and cold rolling dependence of tensile strength and ductility in high nitrogen nickel-free austenitic stainless steel

Gui-Xun Sun(孙贵训), Yue Jiang(江月), Xiao-Ru Zhang(张晓茹), Shi-Cheng Sun(孙世成), Zhong-Hao Jiang(江忠浩), Wen-Quan Wang(王文权), Jian-She Lian(连建设)
Chin. Phys. B, 2017, 26 (**9**): 096104. DOI: 10.1088/1674-1056/26/9/096104

Effects of cold rolling deformation on microstructure, hardness, and creep behavior of high nitrogen austenitic stainless steel

Sun Shi-Cheng (孙世成), Sun Gui-Xun (孙贵训), Jiang Zhong-Hao (江忠浩), Ji Chang-Tao (季长涛), Liu Jia-An (刘家安), Lian Jian-She (连建设)
Chin. Phys. B, 2014, 23 (**2**): 026104. DOI: 10.1088/1674-1056/23/2/026104

SPECIAL TOPIC — Structures and properties of materials under high pressure

Strain rate effects on pressure-induced amorphous-to-amorphous transformation in fused silica

Wenhao Song(宋文豪)[1], Bo Gan(甘波)[1], Dongxiao Liu(刘东晓)[2], Jie Wu(吴杰)[1], Martin T. Dove[1], and Youjun Zhang(张友君)[1,3,†]

[1] *Institute of Atomic and Molecular Physics, Sichuan University, Chengdu* 610065, *China*

[2] *National Key Laboratory of Plasma Physics, Laser Fusion Research Center (LFRC), Chinese Academy of Engineering Physics, Mianyang* 621900, *China*

[3] *Key Laboratory of High Energy Density Physics and Technology of Ministry of Education, Sichuan University, Chengdu* 610065, *China*

(Received 28 December 2024; revised manuscript received 2 February 2025; accepted manuscript online 7 February 2025)

Fused silica (SiO_2 glass), a key amorphous component of Earth's silicate minerals, undergoes coordination and phase transformations under high pressure. Although extensive studies have been conducted, discrepancies between theoretical and experimental studies remain, particularly regarding strain rate effects during compression. Here, we examine strain rate influences on the shock-induced amorphous–amorphous phase transitions in fused silica by measuring its Hugoniot equation of state and longitudinal sound velocity (C_L) up to 7 GPa at strain rates of 10^6–10^7 s^{-1} using a one-stage light-gas gun. A discontinuity in the relationship between shock velocity (U_S) and particle velocity (U_P) and a significant softening in C_L of fused silica were observed near $\sim$ 5 GPa under shock loading. Our results indicate that high strain rates restrict Si–O–Si rotation in fused silica, modifying their bonds and increasing silicon coordination. The transition pressure by shock compression is significantly higher than that under static high-pressure conditions (2–3 GPa), which agrees with some recent theoretical predictions with high compression rates, reflecting the greater pressure needed to overcome energy barriers with the strain rate increase. These findings offer insights into strain rate-dependent phase transitions in fused silica and other silicate minerals (e.g., quartz, olivine, and forsterite), bridging gaps between theoretical simulations and experiments.

Keywords: fused silica, shock compression, phase transition kinetics, strain rate

PACS: 61.43.Fs, 64.70.P–, 91.60.Gf, 91.60.Hg

DOI: 10.1088/1674-1056/adb38f **CSTR:** 32038.14.CPB.adb38f

1. Introduction

SiO_2 is one of the most abundant minerals on the Earth's surface, making its high pressure–temperature (P–T) behavior and physical properties a subject of significant interest in Earth and planetary science.[1,2] Numerous polymorphs of SiO_2, including glass, coesite, and stishovite, have been identified under high P–T conditions through theoretical simulations and experiments for over six decades.[3–6] Fused silica, the amorphous form of SiO_2, represents a critical silicate melt phase in Earth's deep interior. Understanding its phase diagram and transformation kinetics under extreme conditions is essential for advancing knowledge in fundamental physics and geophysics.[7–14]

High P–T experiments and simulations have revealed a variety of phase transformations in fused silica, leading to significant changes in its physical, mechanical, and chemical properties.[15–18] The Si–O coordination number refers to the number of oxygen (O) atoms directly bonded with silicon (Si) atoms within the crystal structure. Notably, changes in the coordination number are a key physical parameter in the amorphous transformation process. For instance, static high-pressure experiments using diamond anvil cells (DACs) identified unusual physical properties at pressures around 3 GPa, likely linked to amorphous-to-amorphous transformations involving Si–O coordination number changes.[19–23] These findings, however, are at odds with theoretical simulations, which predict such transformations, specifically the transition of silicon atoms from fourfold to fivefold coordination, at $\sim$ 5 GPa.[24–26] Meanwhile, similar results were observed in the shock compression experiments, marked by a slope change in the Hugoniot curve at about 5 GPa, indicating the possibility of amorphous transformation. These discrepancies suggest that strain rate, a key variable between static and dynamic compression experiments, may play a critical role in influencing the transformation pathways.

Previous studies have demonstrated that the amorphous transformations in fused silica are influenced by temperature, strain rate, and compression duration. Different compression techniques result in distinct transformation pathways, but the reasons underlying these differences remain unclear. Strain rate, in particular, has been shown to significantly affect the high-pressure mechanical behavior of glassy materials. For instance, under high strain rates, fused silica exhibits increased compressive strength and energy absorption.[27] Shock wave

†Corresponding author. E-mail: zhangyoujun@scu.edu.cn

© 2025 Chinese Physical Society and IOP Publishing Ltd. All rights, including for text and data mining, AI training, and similar technologies, are reserved.

compressions, such as high-speed impact, explosive, and powerful laser, are characterized by strain rates (10^6–10^9 s^{-1}) between static compression (10^{-1}–10^{-2} s^{-1}) and some theoretical simulations (10^8–10^{10} s^{-1}), which provides a unique opportunity to bridge the gap between these approaches and clarify the strain rate effects on amorphous transitions.

In this study, we investigated the equation of state and sound velocity of fused silica up to 7 GPa by shock wave compression. We identified an amorphous–amorphous transition from SiO_4 to SiO_4–SiO_5 structures at a shock pressure of $\sim$ 5 GPa. This transition occurs at higher pressures than static compression experiments but aligns with theoretical predictions overall. By analyzing the effect of strain rate on amorphous transformations of fused silica, we elucidate the mechanisms governing phase transition energy absorption and structural evolution under dynamic conditions. These findings resolve discrepancies between static and dynamic experiments and provide insights into the strain rate-dependent phase transition behavior of silicates.

2. Experimental methods

The fused silica sample, with a density of 2.201(2) g/cm^3 as determined by the Archimedean method, was purchased from PrMat (Shanghai) Co. Ltd. Its purity is 99.9% and porosity is 0. The longitudinal wave (C_L) and shear wave (C_S) sound velocities of the starting sample at ambient conditions were measured to be 5.945(2) km/s and 3.757(2) km/s, respectively, using ultrasonic techniques.[28] The samples were machined into a disc with a diameter of 20 mm and thickness of 2 mm, then polished to optical quality before experimentation.

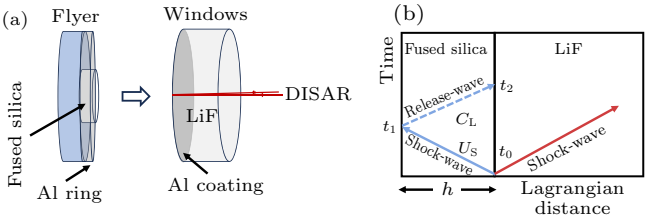


Fig. 1. Schematic representation of the target assemblage for the reverse-impact shock experiments. (a) Experimental configuration for longitudinal sound velocity measurements. The LiF window is impacted by a composite flyer composed of fused silica and aluminum rings. A thin 10-μm-thick aluminum foil is pre-coated to the impact surface of the LiF window to mitigate the effects of stray light. Particle velocities at the fused silica/LiF interface are measured using a DISAR system. (b) Schematic time–distance diagram for the propagation of shock and rarefaction waves in the Lagrange coordinate system on impact. Here, h is the thickness of the sample, U_S is the shock wave velocity, C_L is the rarefaction wave velocity, and t and t_2 are the arrival times of the shock wave and the rarefaction wave at the fused silica/LiF interface, respectively.

Shock compression experiments were carried out using a 24-mm-bore one-stage light-gas gun at the Institute of Atomic and Molecular Physics, Sichuan University. A reverse-impact configuration was employed to simultaneously measure the particle velocity and sound velocity of fused silica at high P–T, as shown in Fig. 1(a). Single-crystal lithium fluoride (LiF) with [100] orientation, 15 mm in diameter and 5 mm in thickness, served as the window material, with aluminum foil coating on its front surface. Flyer velocity (W) was measured using an electromagnetic method within 0.5% uncertainty.[29] The particle velocity profile at the impact interface was recorded using an all-fiber displacement interferometer system for any reflector (DISAR).[30] Figure 1(b) shows the principle for wave interactions between fused silica and LiF during the impact process.

Seven reverse impact experiments were carried out and the Hugoniot density and sound velocity of fused silica were obtained under shock wave compression. The high-speed impact generates shock waves, loading the sample to high P–T states at strain rates up to 10^6–10^7 s^{-1} . These experiments yielded the shock wave velocity, particle velocity, longitudinal sound velocity, bulk sound velocity, bulk modulus, and other parameters for fused silica over a pressure range of 2–7 GPa.[31]

3. Results and discussion

3.1. Amorphous–amorphous transformation of fused silica under shock compression

The relationship between U_S and U_P in condensed matter under shock compression can be typically described by a linear equation within a single phase: $U_S = C_0 + \lambda U_P$, where C_0 and λ are fitted parameters. Our experimental results, combined with previous data,[3,32] reveal a distinct change in the slope of the U_S–U_P relationship, indicating a phase transition. Specifically, the low-pressure phase is characterized by $C_0 = 5.85(4)$ (km/s) and $\lambda = -1.21(11)$, whereas the high-pressure phase exhibits $C_0 = 5.26(6)$ (km/s) and $\lambda = -0.11(9)$. These findings are closely consistent with previous studies.[3,5,6,32–37] Furthermore, the U_S–U_P relationship enables the derivation of the Hugoniot equation of state and the construction of the P_H–ρ curve[38,39]

$$\frac{\rho_H}{\rho_0} = \frac{U_S}{U_S - U_P}, \tag{1}$$

$$P_H = \frac{\rho_0 C_0^2 \left(1 - \frac{\rho_0}{\rho H}\right)}{\left[1 - \lambda\left(1 - \frac{\rho_0}{\rho H}\right)\right]^2}, \tag{2}$$

where ρ_0, ρ_H, and P_H represent the initial density, Hugoniot density, and shock pressure, respectively. As shown in Fig. 3, both the U_S–U_P and P_H–ρ curves for fused silica exhibit a pronounced kink at $\sim$ 5.1 GPa.

Hasmy *et al.*[7] utilized percolation theory to simulate the coordination number transformation in amorphous fused silica under high pressure within 1 ns ($\sim$ 20 GPa/ns), reporting the emergence of substantial SiO_5 polyhedral populations between 3 GPa and 8 GPa. Similarly, Ryuo *et al.*[26] employed

first-principles calculations to analyze Si^5 abundance and observed a sudden increase at ~ 5 GPa, consistent with our experimental results. These observations strongly suggest that fused silica undergoes an amorphous–amorphous phase transition at this pressure, corroborating both theoretical and experimental insights.

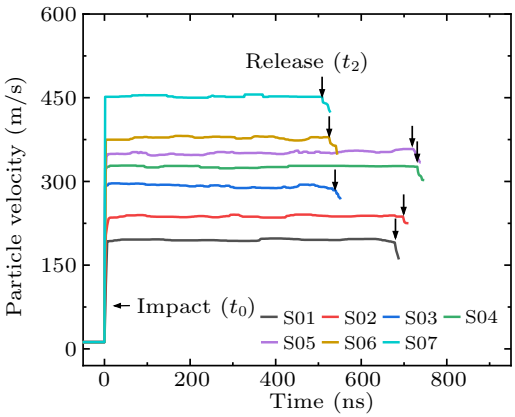


Fig. 2. Measured particle velocity wave profiles at the fused silica/LiF interface upon reverse impact. The times when the shock wave and rarefaction wave reach the fused silica/LiF interface are denoted as t_0 and t_2, respectively. Numbers represent different shots.

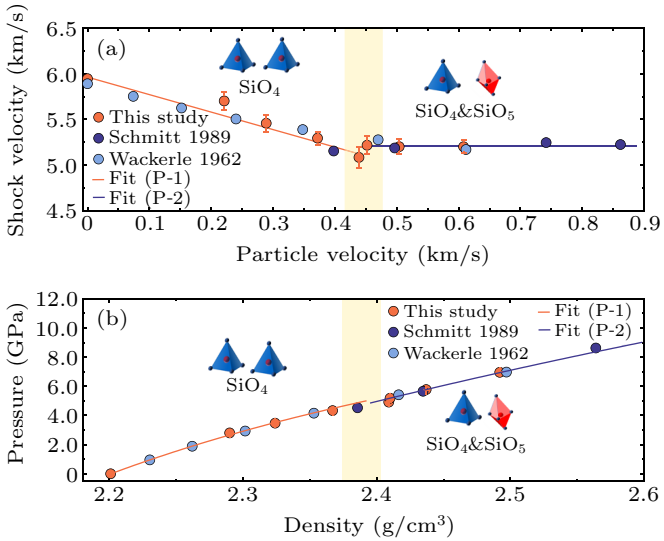


Fig. 3. Hugoniot equation of state of fused silica under shock compression. The orange solid line represents the fitting curve of the low-pressure phase (P-1), while the blue solid line represents the fitting curve of the high-pressure phase (P-2). (a) The relationship between shock velocity (U_S) and particle velocity (U_P). (b) The relationship between Hugoniot pressure (P_H) and density (ρ_H).

3.2. Sound velocity of fused silica across the amorphous–amorphous transition

Change in the sound velocities of condensed matter is one of the most sensitive physical properties for detecting phase transformations.[40] In this study, the Euler longitudinal sound velocity can be obtained by

$$C_L = \left(\frac{\rho_0}{\rho}\right)\frac{h}{(t_2 - t_0) - \dfrac{h}{U_S}}, \tag{3}$$

where h represents the thickness of the sample, and t_0 and t_2 are the arrival times of the shock wave and the rarefaction wave at the fused silica/LiF interface, respectively.

Our experimental results indicate that the C_L of fused silica decreases gradually up to 5 GPa. This negative relationship between C_L and P_H in the low-pressure phase of fused silica can be explained by existing models.[41] The low-pressure phase is well known to consist of short-range ordered SiO_4 tetrahedra.[24] Under shock compression, the SiO_4 tetrahedra could undergo rotation. This rotation causes a change in the oxygen bond angle of the Si–O–Si system, resulting in the bulk modulus tending towards the minimum value.[42,43] Beyond 5 GPa, a significant turning of the sound velocity is observed (Fig. 4). This anomalous behavior indicates a phase transition in the sample, which closely corresponds to the transition pressure indicated by the equation of state. At this pressure, these rotations are restricted, inducing strain in the Si–O–Si bonds and altering the tetrahedra to pentahedra.[44] The volume change of fused silica becomes more pronounced, resulting in an increased bulk modulus. Macroscopically, this manifests as an increase in the C_L of fused silica. This observation aligns well with the theoretical predictions of transition pressure reported by Hasmy *et al.*[7]

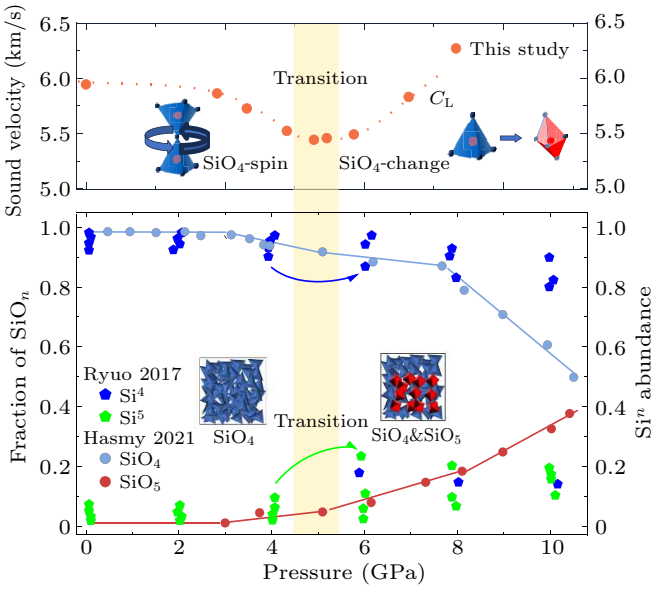


Fig. 4. Measured longitudinal sound velocity (C_L) and the change of coordination number in shock-compressed fused silica. At the shock pressure of ~ 5 GPa, the sound velocity changes and the content of Si^5 and SiO_5 polyhedron significantly increases.

3.3. Effect of strain rate on the amorphous transformation of fused silica

Notably, our shock experimental results display a similar trend in high-pressure sound velocity behavior with that under static compression. However, the transition pressure identified here occurs at approximately 5 GPa, which is about 60% higher than the transition pressure reported under static compression conditions.[20,21] Differences in the shock tempera-

ture and strain rate are likely the key factors contributing to this discrepancy. To account for these effects, we employed a thermodynamical approach to estimate the shock temperature of fused silica along the Hugoniot[31]

$$\mathrm{d}T = -T\left(\frac{\gamma}{V}\right)\mathrm{d}V + \left(\frac{1}{2C_V}\right) \times [(V_0 - V)\mathrm{d}P + (P - P_0)\mathrm{d}V], \quad (4)$$

where γ refers to the effective Grüneisen parameter, V_0 and V are the specific volumes at ambient conditions and under shock compression, respectively, and C_V is the specific heat capacity.

Compared to the static compression experiment temperature of $\sim$ 300 K, the estimated shock temperature only increases less than 50 K up to 7 GPa (Table 1), so the temperature effect can be negligible. Consequently, the observed discrepancies are likely attributable to variations in strain rate. Strain rate (ε) is calculated using the formula[45]

$$\varepsilon = \frac{\rho_\mathrm{H}}{\rho_0 C_\mathrm{L}} \frac{\mathrm{d}U_\mathrm{P}}{\mathrm{d}t}. \quad (5)$$

The strain rate of fused silica in these shock experiments is estimated to range from 10^6 s^{-1} to 10^7 s^{-1} (Table 1), which is closer to the strain rates in theoretical simulations ($\sim 10^8$–10^{10} s^{-1}, for example, the compression rate of $\sim$ 20 GPa/ns.[7]) It is approximately 8 to 9 orders of magnitude higher than that under static compression (10^{-2} s^{-1}).[20] The high strain rate characteristics are typically associated with more rapid pressure increases, making these differences critical factors in explaining the observed discrepancies between the results obtained from static experiments and simulations of fused silica.

Table 1. Impact conditions and experimental results for fused silica under shock compression.

Shot No.	W (km/s)	U_P (km/s)	U_S (km/s)	P_H (GPa)	ρ_H (g/cm^3)	C_L (km/s)	C_B (km/s)	K_S (GPa)	T_est (K)	ε (s^{-1})
S1	0.416(2)	0.221(2)	5.73(8)	2.80(1)	2.290(2)	5.78(17)	3.83(17)	33(5)	316(2)	6.2×10^6
S2	0.526(2)	0.289(2)	5.46(7)	3.47(2)	2.324(2)	5.73(13)	3.36(10)	26(5)	320(2)	8.3×10^6
S3	0.664(2)	0.372(3)	5.29(5)	4.33(3)	2.367(2)	5.52(13)	3.46(22)	28(5)	325(3)	1.1×10^7
S4	0.768(2)	0.439(4)	5.08(9)	4.91(5)	2.409(5)	5.44(12)	3.37(18)	27(5)	333(3)	1.3×10^7
S5	0.798(3)	0.452(5)	5.22(9)	5.18(7)	2.410(7)	5.46(12)	3.66(17)	32(6)	335(3)	1.4×10^7
S6	0.886(4)	0.504(4)	5.20(8)	5.77(5)	2.437(5)	5.49(18)	3.71(11)	33(4)	339(3)	1.6×10^7
S7	1.060(7)	0.608(4)	5.19(6)	6.95(5)	2.492(5)	5.83(17)	4.20(10)	44(4)	347(3)	1.8×10^7

Note: ρ_0 is the initial density of fused silica at ambient pressure; W is the measured flyer velocity; U_S and U_P are the shock velocity and particle velocity, respectively; P_H and ρ_H are the Hugoniot pressure and density, respectively; C_L and C_B are the Eulerian longitudinal sound velocity and Eulerian bulk sound velocity, respectively, which are calculated by formula (3) and Refs. [56–59]; K_S is the calculated bulk modulus; T_est is the estimated shock wave temperature given by Eq. (4); ε is the strain rate given by Eq. (5). The Hugoniot parameters used in the study are given as: LiF, $\rho_0 = 2.640(0.002)$ g/cm^3, U_S (km/s) $= 5.215(0.02) + 1.351(0.03)U_\mathrm{P}$ (km/s).[60]

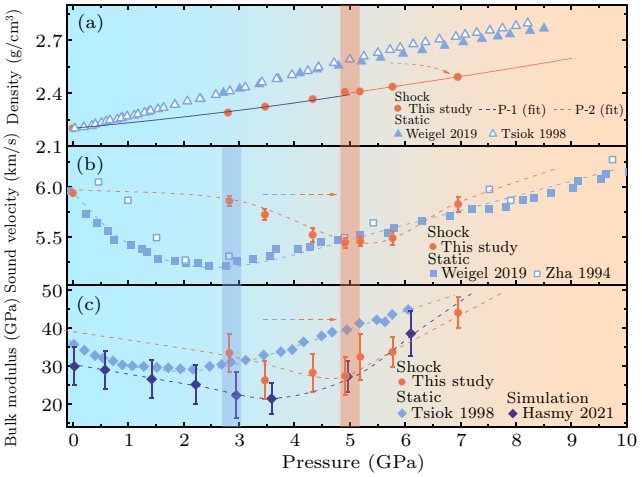


Fig. 5. Comparisons of density, sound velocity, and bulk modulus in fused silica under high pressure among static, shock experiments, and theoretical simulation. (a) The densification of fused silica under high strain rates is significantly lower compared to that at low strain rate conditions. The transition pressure in the longitudinal sound velocity (b) and bulk modulus (c) of fused silica shifts towards higher-pressure regions at higher strain rates.

The shock experimental results for fused silica are compared with those obtained from static compression experiments and theoretical simulations. Significant discrepancies are observed in the pressure–density (P–ρ) relationship of fused silica under varying strain rates (Fig. 5(a)). These differences can be attributed to the viscoelastic behavior of fused silica which involves relaxation processes during densification under high pressure.[46] Phase transitions in viscoelastic materials typically require sufficient time to overcome energy barriers. However, under shock compression and theoretical simulation, the rapid pressure increase at high strain rates limits the completion of these relaxation processes, resulting in lower densities achieved under high strain rates compared to those obtained under static high-pressure conditions. A similar phenomenon has also been observed in the P–ρ relationship of other viscoelastic solids, such as Al_2O_3.[47–50]

Previous studies have shown that strain rates and compression duration significantly influence both the amorphous–amorphous transformation and the compressive strength of fused silica.[12,27] Building on these findings, we optimized an empirical formula to describe the absorption energy during amorphous–amorphous transitions as a function of strain rate and pressure

$$E = \int_{x_{i-1}}^{x_{i+1}} kP(x)\,\mathrm{d}x = \frac{x}{2}k'[P(x_{i-1}) + 2P(x_i) + P(x_{i+1})], \quad (6)$$

where Δx is the strain variable, which is highly correlated with

strain rate and duration, and macroscopically manifested as a change in specific volume, k is an empirical parameter, and $P(x_i)$ denotes the integral of pressure, influenced by strain rate and pressure.

In Eq. (6), we present three-dimensional plots to illustrate the absorption energy of fused silica as a function of specific volume and pressure on the amorphous transition under strain rates (Figs. 6(b) and 6(c)). Despite the higher strain rates under dynamic compression, there is a less pronounced discrepancy in specific volumes between shock and static compression. As a result, achieving amorphous transformation and overcoming the phase transition barrier require higher shock pressure to provide the necessary driving force for the transition.[46] These observations, along with variations in sound velocity and pressure hysteresis in fused silica under shock compression, can be reasonably attributed to this phenomenon.

The pressure-induced amorphous-to-amorphous phase transition in fused silica is linked to the contraction of short-range ordered ring structures (Fig. 6(a)), a process that requires finite time.[51] Therefore, in high-strain-rate shock experiments and theoretical simulations, the formation of a high-pressure phase in fused silica is hindered by the rapid strain rate and short duration. This results in a mixed state where different amorphous structures coexist. In contrast, static compression, with its longer duration, allows sufficient time for crystallization and the formation of a high-pressure phase. This discrepancy between shock and static high-pressure behavior is also observed in other silicate minerals, such as single-crystal α-quartz and olivine.[52–55] This work presents a promising avenue for further exploration of this issue.

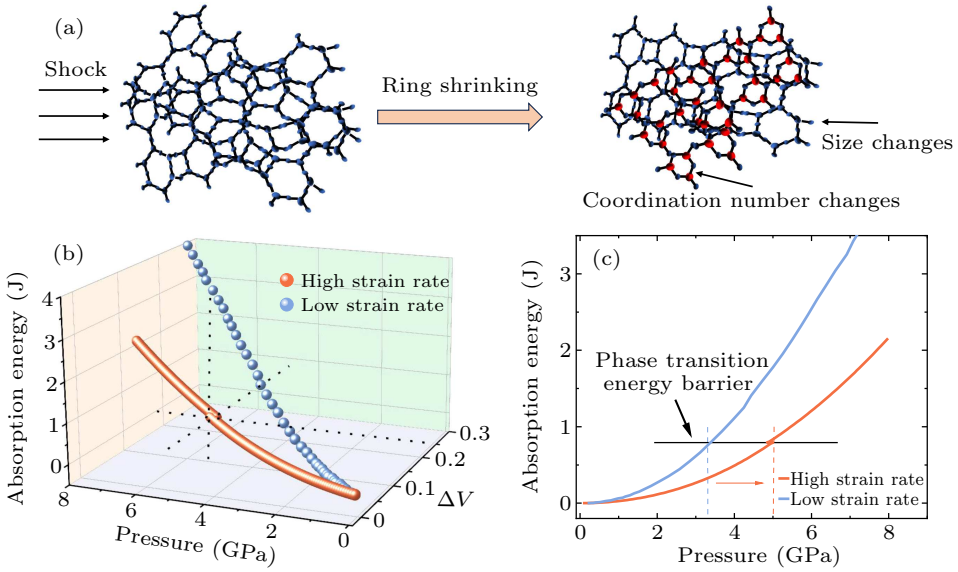


Fig. 6. Proposed amorphous–amorphous phase transformation in compressed-fused silica. (a) Schematic diagram of the coordination number change of fused silica under shock compression. (b) Relationship among absorbed energy, volume strain (ΔV), and pressure at different strain rates and (c) its cross-sectional view.

4. Summary and conclusions

This study explores the phase transformation of fused silica under shock compression within the pressure range of 2–7 GPa under high strain rates. The Hugoniot equation of state and longitudinal sound velocity were measured, revealing a pronounced kink at approximately 5 GPa. These findings, in conjunction with prior theoretical simulations, indicate that fused silica undergoes an amorphous–amorphous phase transformation from SiO_4 to SiO_4–SiO_5 structures under shock compression. By comparing results from shock experiments (strain rates of 10^6–10^7 s^{-1}) with those from theoretical simulations (10^8–10^{10} s^{-1}) and static compression (10^{-2} s^{-1}), it is evident that the amorphous–amorphous phase transformation in fused silica is highly strain rate-dependent. Under shock compression, the strain rate is significantly higher, and the duration is much shorter than that under static compression. As a result, achieving the amorphous phase transition requires higher shock pressure to provide the necessary driving force.

Acknowledgements

The authors acknowledge Yang Wang, Luyan Zhou, and Haidong Jin for their help in shock-wave experiments. This work was supported by the National Natural Science Foundation of China (Grant Nos. 42422201, 12175211, and 12350710177) and the Sichuan Science and Technology Program (Grant No. 2023NSFSC1910).

References

[1] Duffy T, Madhusudhan N and Lee K K M 2015 *Treatise on Geophysics* **2** 149
[2] Wu Y, Wang Y, Zhang Y, Jin Z, Wang C and Zhou C 2011 *Chin. Sci. Bull.* **57** 894
[3] Wackerle J 1962 *J. Appl. Phys.* **33** 922
[4] McQueen R, Fritz J and Marsh S 1963 *Journal of Geophysical Research* **68** 2319

[5] McQueen R 1968 *Seismic Coupling. Proceedings of a meeting sponsored by the Advanced Research Projects Agency at Stanford Research Institute*, Menlo Park, California, pp. 15–16
[6] Green S, Isbell W, Jones A, Maiden C, Perkins R and Shipman F 1968 *Material Properties Measurements for Selected Materials*, NASA-CR-73230
[7] Hasmy A, Ispas S and Hehlen B 2021 *Nature* **599** 62
[8] Langenhorst F 2024 *Nature Geoscience* **17** 592
[9] Lu H B 2024 *Reports on Progress in Physics* **87** 032601
[10] Berryman E J, Winey J M, Gupta Y M and Duffy T S 2019 *Geophysical Research Letters* **46** 13695
[11] Gleason A E, Bolme C A, Lee H J, Nagler B, Galtier E, Milathianaki D, Hawreliak J, Kraus R G, Eggert J H, Fratanduono D E, Collins G W, Sandberg R, Yang W and Mao W L 2015 *Nat. Commun.* **6** 8709
[12] Tracy S J, Turneaure S J and Duffy T S 2018 *Phys. Rev. Lett.* **120** 135702
[13] Gleason A E, Bolme C A, Lee H J, Nagler B, Galtier E, Kraus R G, Sandberg R, Yang W, Langenhorst F and Mao W L 2017 *Nat. Commun.* **8** 1481
[14] Alexander C S, Chhabildas L C, Reinhart W D and Templeton D W 2008 *International Journal of Impact Engineering* **35** 1376
[15] Haines J, Leger J M, Gorelli F and Hanfland M 2001 *Phys. Rev. Lett.* **87** 155503
[16] Bykova E, Bykov M, Cernok A, Tidholm J, Simak S I, Hellman O, Belov M P, Abrikosov I A, Liermann H P, Hanfland M, Prakapenka V B, Prescher C, Dubrovinskaia N and Dubrovinsky L 2018 *Nat. Commun.* **9** 4789
[17] Hu Q Y, Shu J F, Cadien A, Meng Y, Yang W G, Sheng H W and Mao H K 2015 *Nat. Commun.* **6** 6630
[18] Ono S, Kikegawa T, Higo Y and Tange Y 2017 *Physics of the Earth and Planetary Interiors* **264** 1
[19] Tsiok O B, Brazhkin V V, Lyapin A G and Khvostantsev L G 1998 *Phys. Rev. Lett.* **80** 999
[20] Weigel C, Mebarki M, Clement S, Vacher R, Foret M and Ruffle B 2019 *Phys. Rev. B* **100** 094102
[21] Zha C, Hemley R J, Mao H, Duffy T S and Meade C 1994 *Phys. Rev. B* **50** 13105
[22] Neyer B T 1987 *Proc. SPIE* **648** 301
[23] Duffy T S and Ahrens T J 1995 *Journal of Geophysical Research: Solid Earth* **100** 529
[24] Trachenko K and Dove M T 2003 *Phys. Rev. B* **67** 064107
[25] Trachenko K, Dove M T, Brazhkin V and El'kin F S 2004 *Phys. Rev. Lett.* **93** 135502
[26] Ryuo E, Wakabayashi D, Koura A and Shimojo F 2017 *Phys. Rev. B* **96** 054206
[27] Daryadel S S, Mantena P R, Kim K, Stoddard D and Rajendran A M 2016 *J. Non-Crystalline Solids* **432** 432
[28] Ohtsuka Y 1973 *J. Phys. E Sci. Instrum.* **6** 868
[29] Li X H, Yang C, Gan B, Huang Y Q, Wang Q M, Sekine T, Hong J W, Jiang G and Zhang Y J 2022 *Phys. Rev. B* **105** 104110
[30] Weng J D, Tan H, Wang X, Ma Y, Hu S L and Wang X S 2006 *Appl. Phys. Lett.* **89** 111101
[31] Huang Y Q, Hou M Q, Gan B, Li X H, He D W, Jiang G, Zhang Y J and Liu Y 2022 *Journal of Geophysical Research-Solid Earth* **127** 11
[32] Schmitt D R and Ahrens T J 1989 *Journal of Geophysical Research* **94** 5851
[33] Ahrens T J and Johnson M L 1995 *Mineral Physics & Crystallography* pp. 143–184
[34] Kondo K-i, Ahrens T J and Sawaoka A 1983 *J. Appl. Phys.* **54** 4382
[35] Lyzenga G A and Ahrens T J 1980 *Geophysical Research Letters* **7** 141
[36] Marsh S P 1980 *LASL shock Hugoniot data* (University of California Press)
[37] Schmitt D, Svendsen B and Ahrens T J 1986 *Shock Waves in Condensed Matter*, Gupta Y M ed. (Boston, MA: Springer US) pp. 261–265
[38] Mitchell A and Nellis W 1981 *J. Appl. Phys.* **52** 3363
[39] Gan B, Jiang G, Huang Y Q, Zhang H, Hu Q Y and Zhang Y J 2023 *Phys. Rev. B* **107** 064106
[40] Zhou L, Jiang G, Gan B, Zhuang Y, Zhang H and Zhang Y 2023 *J. Appl. Phys.* **133** 14
[41] Vukcevich M R 1972 *J. Non-Crystal. Solids* **11** 25
[42] Grimsditch M 1984 *Phys. Rev. Lett.* **52** 2379
[43] Kondo K, Lio S and Sawaoka A 1981 *J. Appl. Phys.* **52** 2826
[44] Meade C and Jeanloz R 1987 *Phys. Rev. B* **35** 236
[45] Smith R, Minich R, Rudd R, Eggert J, Bolme C, Brygoo S, Jones A and Collins G 2012 *Phys. Rev. B* **86** 245204
[46] Kim H, Hambir S A and Dlott D D 2000 *Journal of Physical Chemistry B* **104** 4239
[47] Schuler K W, Nunziato J W and Walsh E K 1973 *Int. J. Solids Struct. (UK)* **9** 1237
[48] Telfair D 1954 *J. Appl. Phys.* **25** 1062
[49] Banishev A A, Shaw W L, Curtis A D and Dlott D D 2014 *Appl. Phys. Lett.* **104** 101914
[50] Grady D E 1980 *Journal of Geophysical Research* **85** 913
[51] Renou R, Soulard L, Lescoute E, Dereure C, Loison D and Guin J-P 2017 *The Journal of Physical Chemistry C* **121** 13324
[52] Syono Y, Goto T, Takei H, Tokonami M and Nobugai K 1981 *Science* **214** 177
[53] Langenhorst F, Boustie M, Migault A and Romain J 1999 *Earth and Planetary Science Letters* **173** 333
[54] Poirier J, Peyronneau J, Madon M, Guyot F and Revcolevschi A 1986 *Nature* **321** 603
[55] Zhang J S and Bass J D 2016 *Geophysical Research Letters* **43** 9611
[56] Zhang Y J, Sekine T, He H L, Yu Y, Liu F S and Zhang M J 2016 *Scientific Reports* **6** 22473
[57] Duffy T S and Ahrens T J 1992 *Journal of Geophysical Research: Solid Earth* **97** 4503
[58] Barron T H K, Collins J F, Smith T W and White G K 1982 *J. Phys. C Solid State Phys.* **15** 4311
[59] Petrovtsev A V 2006 *AIP Conference Proceedings* **849** 380
[60] Rigg P A, Knudson M D, Scharff R J and Hixson R S 2014 *J. Appl. Phys.* **116** 033515